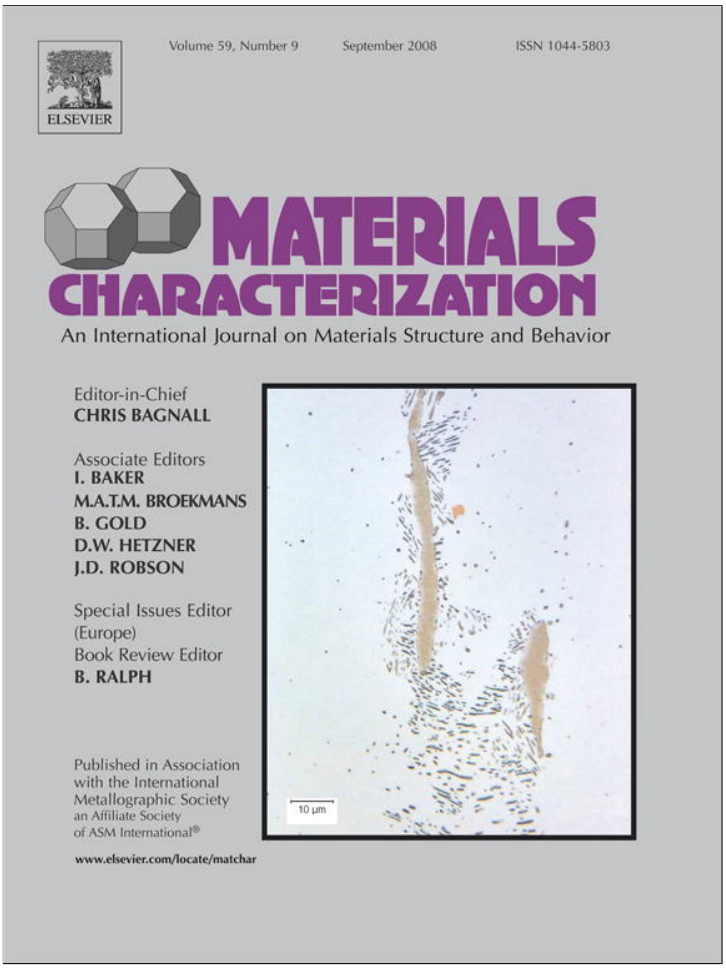

MATERIALS CHARACTERIZATION 59 (2008) 1342–1348

Examination of the solidification macrostructure of spheroidal and flake graphite cast irons using DAAS and ESBD

G. Rivera[a], *P.R. Calvillo*[b], *R. Boeri*[a,*], *Y. Houbaert*[b], *J. Sikora*[a]

[a]*Metallurgy Division INTEMA, National University of Mar del Plata, CONICET, J. B. Justo 4302 (B7608FDQ) Mar del Plata, Argentina*
[b]*Department of Metallurgy and Materials Science, Ghent University, Belgium*

ARTICLE DATA

Article history:
Received 19 October 2007
Received in revised form 21 November 2007
Accepted 30 November 2007

Keywords:
Macrostructure
Cast iron
DAAS, EBSD

ABSTRACT

This investigation focuses on the study of the solidification macrostructure of sand cast flake and spheroidal graphite cast irons. The macrostructure is revealed by using a special technique developed earlier by the authors, called Direct Austempering After Solidification. The observations make use of conventional metallography and Electron Back Scattering Diffraction. The latter technique allows a more detailed observation of the morphology of the austenite grains and the microstructure of the matrix. The results of Electron Back Scattering Diffraction validate the observations made using the macrographic technique. It is verified that the solidification of both flake and spheroidal graphite cast irons is dominated by the growth of large austenite dendrites that form a grain pattern similar to that usually found in most metallic alloys.

1. Introduction

Flake graphite cast iron (FGI) and spheroidal graphite cast iron (SGI) are extensively used in the fabrication of parts for several industries. As for every cast material, proper knowledge of their solidification is necessary to optimize mold filling and parts soundness, and to obtain the desired microstructures. Nevertheless, there is no universally accepted explanation of the solidification mechanisms of these materials. The most noticeable disagreements among different explanations refer to the morphology taken by the austenite as the solidification advances. The final morphology of graphite precipitates is easily observed by metallography. On the other hand, the morphology of the primary austenite is hindered by the solid state transformations suffered by the austenite as it cools below the eutectoid temperature. It is generally agreed that the pro-eutectic austenite grows dendritically in hypoeutectic cast irons. Nevertheless, most explanations of the solidification of FGI pay little attention to the role of austenite dendrites in eutectic and hypereutectic alloys. The most broadly accepted explanation of the solidification of FGI states that eutectic solidification units are formed by nearly spherical aggregates of austenite and graphite growing cooperatively, producing the so called "eutectic cells" [1–5]. On the other hand, the solidification of SGI was very often pictured as dominated by the independent growth of units formed by single graphite nodules surrounded by austenite [6–8]. It is now apparent that these mechanisms are incorrect. In fact, recent investigations of the authors have shown that a special procedure, called DAAS (Direct Austempering After Solidification), can be used to reveal the solidification macrostructure of free graphite cast irons [9,10]. Through this technique the solidification macrostructure of FGI and SGI have been found to be dominated by the growth of relatively large dendrites of austenite that give rise to a grain structure very similar to that usually found in most metallic alloys. The unexpected presence of large austenite dendrites in hypereutectic compositions was also shown [9–14]. These findings verified the results of earlier studies that warned about the presence of austenite dendrites in free graphite cast irons, but were not able to bring up conclusive evidences of their morphology and extension [2,3,15–19]. In spite of the evidences regarding the

* *Corresponding author*. Tel.: +54 223 4816600; fax: +54 223 4810046.
E-mail addresses: boeri@fi.mdp.edu.ar (R. Boeri), jsikora@fi.mdp.edu.ar (J. Sikora).

1044-5803/$ – see front matter © 2007 Elsevier Inc. All rights reserved.
doi:10.1016/j.matchar.2007.11.009

Fig. 1 – Solidification macrostructure of flake graphite cast iron revealed by DAAS and chemical etching. Light macroscopy.

role of austenite dendrites, many computational models that aim to calculate cast iron solidification are based on approaches that neglect the dendritic growth of austenite. Therefore, the conclusions drawn from the calculations of those models lack of a physical support and are insufficiently accurate.

The typical result of the application of DAAS technique on a 20 mm sand cast round bar of near eutectic gray iron is shown in Fig. 1. DAAS technique is described briefly in the experimental methods section. A grain structure is clearly seen after the sample is etched with Picral 4%. Nevertheless, the observation and differentiation of grains are not simple. Different grains become distinguishable depending on the type and incidence angle of illumination. As a result, precise counting and measuring of grains becomes difficult. Furthermore, in order for the new explanations of the solidification of FGI and SGI to be universally accepted, it is necessary to bring up additional support to the DAAS technique. For example, as the magnification of macroscopic techniques is limited, and conventional light microscopy cannot be used to look at the austenite grains, the detailed examination of grain boundaries

Table 1 – Chemical composition

Melt	CE (wt%)	C (wt%)	Si (wt%)	Mn (wt%)	Cu (wt%)	Ni (wt%)
F1	4.27	3.28	2.95	0.22	0.93	0.46
F2	4.64	3.61	3.11	0.18	1.05	0.68
S	4.70	3.61	3.27	0.33	0.63	0.59

CE: carbon equivalent.

Table 2 – Graphite characteristics (ASTM A247)

Melt				
	F1	Flake	Type	A
			Size	4
	F2	Flake	Type	C
			Size	4
	S	Spheroidal	Nodularity	100%
			Size	6
			Nodule Count	100 nodules/mm^2

is not possible. To accomplish this task, it would be desirable to count with a higher resolution observation method. The Electron Back Scattering Diffraction (ESBD) is a technique that works attached to a Scanning Electron Microscope, and can be used to recognize crystal orientations of a given phase at the microscopic level. It can be also adapted to reveal grains at the macroscopic level.

The objective of this investigation is to reveal and to characterize the macrostructure of cast irons of different graphite morphologies and carbon equivalents subjected to DAAS using EBSD.

2. Experimental Procedure

All tests were carried out on samples obtained from cast iron heats made at the foundry pilot plant of INTEMA. Melting was carried out by using a medium frequency induction furnace of 50 kg capacity. The chemical compositions are listed on Table 1. Melts F1 and F2 have flake graphite and near eutectic and hypereutectic carbon equivalent, respectively. Melt S is hypereutectic and has spheroidal graphite. The graphite characteristics, according to ASTM A247, are listed in Table 2. All compositions include small amounts of Cu and Ni that were added to reach the level of austemperability needed to carry out the DAAS procedure. Round bars were cast from the melts, using alkydic resin bonded sand molds.

2.1. *DAAS Technique*

The DAAS technique has been described in detail in the literature [9,10]. In order to make it possible to reveal the solidification macrostructure after solidification is complete, a significant portion of the primary austenite must be retained at room temperature. This can be achieved by performing an austempering heat treatment of the cast part during the cooling stage immediately after solidification. To do this, cast

Fig. 2 – Schematic macrostructure showing coloring of grains according to their crystal orientation.

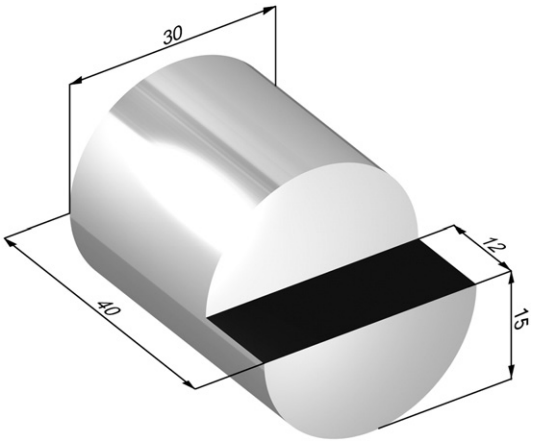

Fig. 3 – Sectioning of the round bars. The black surface was analyzed by ESBD. References are in millimeters.

parts must be shaken out when they are above 900 °C and austempered. The recommended procedure involves a temperature homogenization stage at 920 °C, carried out between shake out and austempering. Austempering is generally done at relatively high temperatures, between 350 and 400 °C, in order to maximize the amount of retained austenite. The austempering heat treatment leads to a matrix microstructure formed by a fine mixture of acicular ferrite and austenite. This austenite, which accounts for about 40% of the volume of the matrix, is in fact the primary austenite, and, after a regular polishing and chemical etching with Picral (4%), reveals the solidification macrostructure, as shown in Fig. 1.

2.2. *EBSD Technique*

EBSD allows obtaining crystallographic information from polished samples using a scanning electron microscope (SEM). The samples were prepared following standard metallography procedures. Final polishing was carried out using colloidal silica of 0.035 μm particle size. As the electron beam of the SEM strikes the surface of a tilted specimen, the electrons are elastically scattered beneath the surface. The diffracted electrons form Kikuchi patterns on a fluorescent

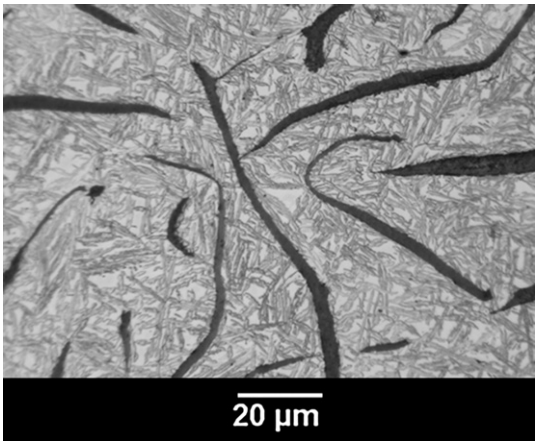

Fig. 4 – Microstructure of sample F1.

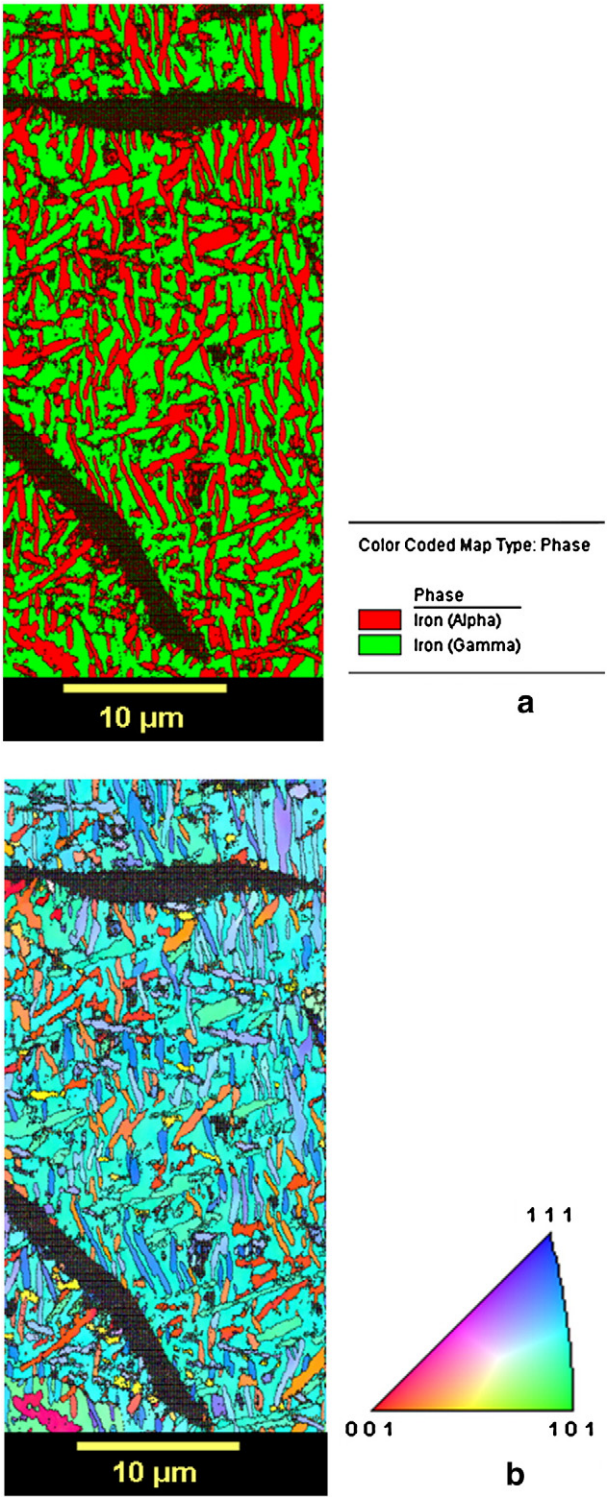

Fig. 5 – Microstructure of sample F1 examined by EBSD, (a) Phase distribution map, (b) Inverse pole figure (IPF) map.

screen, allowing the crystal orientation to be identified. As a polycrystalline sample is scanned by the electron beam, information on the crystalline orientation at each point is obtained [20]. The resulting scans allow revealing the grain morphology and crystal orientation. The samples scanned using the EBSD technique were analyzed with Orientation Imaging Microscopy (OIM). Misorientations below 2° were not

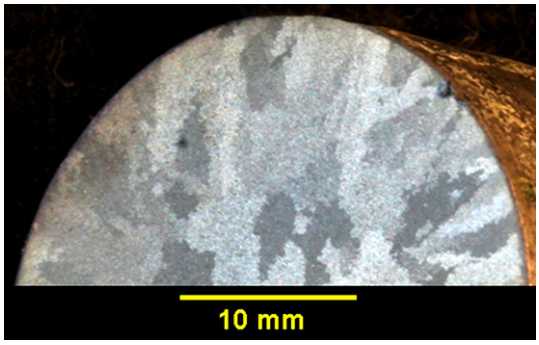

Fig. 6 – Solidification macrostructure of sample F1 revealed by DAAS and chemical etching. Light macroscopy.

considered in data post-processing. Boundaries with misorientation between 2 and 15° were defined as low angle grain boundaries or subgrains and those with misorientations greater than 15° were considered as high angle grain boundaries or grains. Then, each crystalline orientation can be represented in the digitalized image by a different color. As an example, Fig. 2 shows schematically a macrostructure where grains having the [111] axis perpendicular to the surface are shown in blue.

EBSD was used to reveal the grains in round cast bars that were previously subjected to DAAS. Fig. 3 shows a schema of the sectioning of the bars, where studied surfaces are pointed.

The ESBD tests were carried out at the Department of Metallurgy and Materials Science of Ghent University, Belgium. Seven scans of 2.4 by 3.0 mm at steps of 5 μm were carried out on each bar, working under specific microscope conditions to cover large areas by increasing the electron interaction area between samples and the electron beam. The scans covered the section from the centerline to the surface of the rod, as shown in Fig. 3. Additional higher resolution scans, using a 0.5 μm, were carried out to examine the microstructure in detail.

3. Results and Discussion

The microstructure of all samples after austempering is formed by a matrix of acicular ferrite and austenite, usually called ausferrite, and a dispersion of graphite precipitates. Fig. 4 shows the microstructure of sample F1. Fig. 5 shows the microstructure of sample F1 examined by ESBD using a 0.5 μm step scan. Fig. 5a shows the phase distribution map. The background, in green, is austenite, while the red needles are ferrite, and the black areas, which correspond to points not indexed, are graphite. Fig. 5b shows an inverse pole figure (IPF) map, where different colors are assigned to crystals of different orientation. Note that all the austenite in the matrix displays the same color, indicating that the whole background is the same crystal, while the ferrite crystals have different colors. The excellent capabilities of ESBD technique to recognize phases and crystal orientations on cast irons with this microstructure are verified, nevertheless, at this high magnification, the field is smaller than the austenite grains and therefore the macrostructure is not revealed. A larger field must be examined.

Fig. 8 – EBSD map for austenite of sample F1 after DAAS technique. Higher magnification than Fig. 7.

Fig. 6 shows the solidification macrostructure along a transverse section of the cast rod of melt F1, as revealed by DAAS and Picral etching. Small grains are observed near the surface, while the center of the sample shows relatively larger equiaxed grains. Details of the microstructure, such as graphite precipitates, are not visible since the magnification used for macrography is low. It is worth mentioning that macrostructures of sand cast flake graphite irons of regular

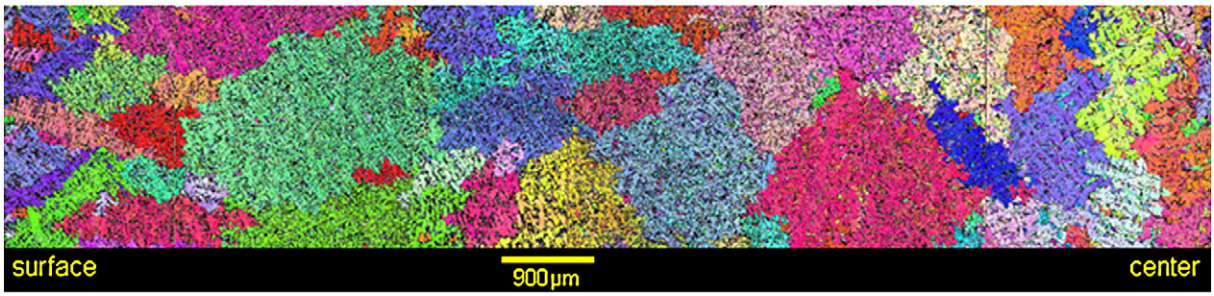

Fig. 7 – EBSD map for austenite of sample F1 after DAAS technique.

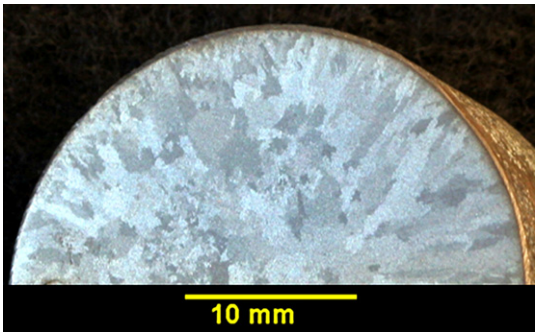

Fig. 9 – Solidification macrostructure of sample F2 revealed by DAAS and chemical etching. Light macroscopy.

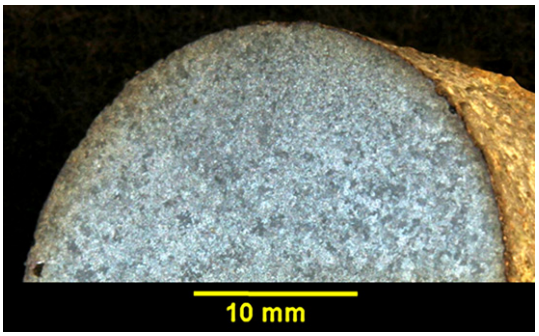

Fig. 10 – Solidification macrostructure of sample S revealed by DAAS and chemical etching. Light macroscopy.

chemical composition, as such shown in Fig. 6, have been rarely shown in the literature, and can be revealed only through the application of DAAS, to the best of our knowledge [9–14,21]. Fig. 7 shows ESBD map for austenite of sample F1. The figure integrates the seven maps obtained into one picture. The grain structure is in coincidence with that shown in Fig. 6 for the same sample. The size of the grains ranges between 2 and 3 mm. The ESBD map shows the macrostructure in better detail than optical metallography. A higher magnification EBSD map for austenite of F1 is shown in Fig. 8. The dark precipitates inside each grain are graphite. The absence of graphite in some regions of the grains allows identifying the dendritic structure of the austenite inside each grain. The way in which growing austenite dendrites interact to form the grain boundaries is also seen. Grain borders are quite irregular and intricate. This suggests that the collision of growing solids takes place at an early stage of solidification, between relatively thin and sparse dendrites. It is apparent that there are no regions of the microstructure that were dominated by other non-dendritic growth mechanisms of austenite.

Figs. 9 and 10 show the macrostructure of the hypereutectic irons F2 and S, respectively, revealed by optical macroscopy. The grain structure of SGI sample S is much finer than that of FGI sample F2. The marked difference in the grain size is confirmed by the examination of the same samples by ESBD, as shown in Figs. 11 and 12. The dark spots, shown in Fig. 12, inside each grain are graphite spheroids. Large differences in the grain size of spheroidal and flake graphite cast irons of similar carbon equivalent, solidified at a similar rate, have been reported earlier [14]. The origin of this difference remains unexplained.

The grain borders in SGI are smoother than those found in FGI. This may indicate that at the time of interaction, the growing units have a more rounded shape than in the case of GI. This may also be affected by the carbon equivalent value. This subject requires further investigation.

The comparison of Figs. 6 and 9 shows that regardless of carbon equivalent, flake graphite cast irons show similar macrostructure, as the solidification is dominated by large austenite dendrites. These findings contradict common knowledge, which assumes that dendritic growth of austenite is prevented in hypereutectic gray cast irons. Based on the current observations, it can be concluded that, within a broad range of carbon equivalent values, the solidification of free graphite cast irons involve the nucleation and dendritic growth of austenite, which continue growing until they define a grain structure.

The results of this study support earlier proposals of the authors about the solidification mechanism of FGI and SGI [9–14]. The solidification mechanisms for eutectic alloys are shown schematically in Fig. 13. In both cases the solidification starts with the independent nucleation of austenite dendrites and graphite from the melt. As heat is extracted austenite dendrites grow and interact with graphite precipitates. The interaction is quite different depending on the graphite morphology. Flake graphite and austenite form units that grow cooperatively, with both phases in contact with the melt. These units are sometimes called “eutectic cells” or “eutectic

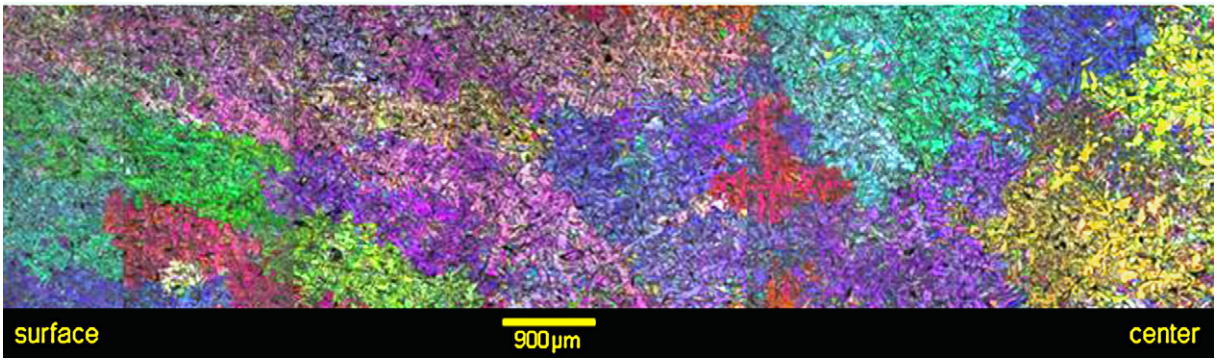

Fig. 11 – EBSD map for austenite of sample F2 after DAAS technique.

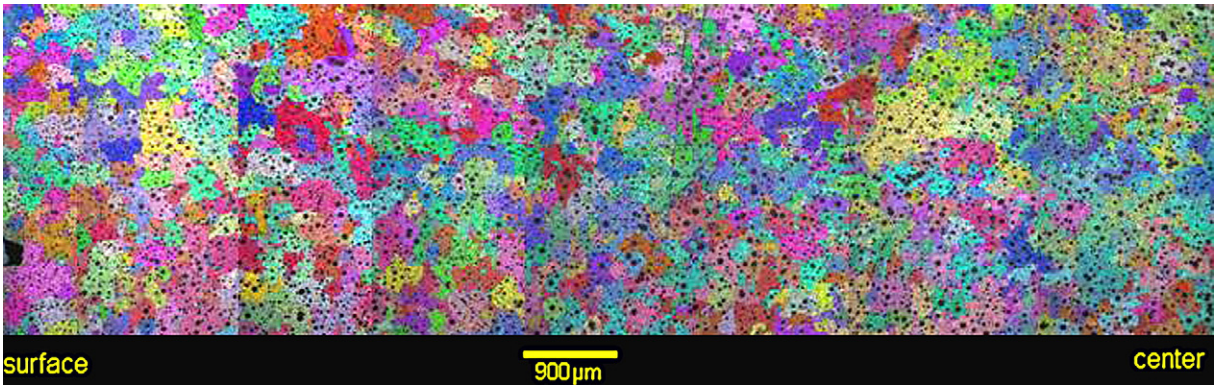

Fig. 12 – EBSD map for austenite of sample S after DAAS technique.

colonies". On the other hand, spheroidal graphite particles are enveloped by an austenite layer soon after they get in contact with the growing austenite dendrites. Further growth of graphite is controlled by the diffusion of carbon from the melt to the graphite through the austenite envelope. As dendrites grow they contact each other, defining the grain size. As a result of this growth mechanism, each austenite grain contains a large number of graphite particles inside.

The proposed solidification mechanism is certainly complex and difficult to be modeled mathematically. Nevertheless, a correct representation of the evolution of the shapes of the growing solids is necessary to predict microsegregation, microstructure and shrinkage formation accurately. Future studies should be addressed to identify the factors controlling grain size and dendrite coarseness in the different types of cast irons.

4. Conclusions

- The use of EBSD on flake and spheroidal graphite cast iron samples treated with Direct Austempering After Solidification successfully reveals their solidification macrostructure.
- ESBD allows the observation of grain boundaries in good detail. Boundaries in flake graphite irons are markedly irregular, suggesting that the interactions between the growing austenite dendrites take place at an early stage of solidification.
- ESBD analysis shows that the solidification of both flake and spheroidal graphite cast irons is dominated by the growth of austenite dendrites that form a grain pattern similar to that usually found in most metallic alloys. This gives additional support to the solidification mechanisms proposed earlier.

Acknowledgements

Financial support from Argentinean institutions UNMDP, CONICET and SECYT, are gratefully recognized.

REFERENCES

[1] Angus H. Cast iron: physical and engineering properties. Butterworth & Co Ltd.; 1976.
[2] Stefanescu D. Cast iron. Metals Handbook, vol. 15. ASM International; 1998.
[3] Morrogh H, Olfield W. Solidification of grey cast iron. Iron Steel 1959;32:431–4.

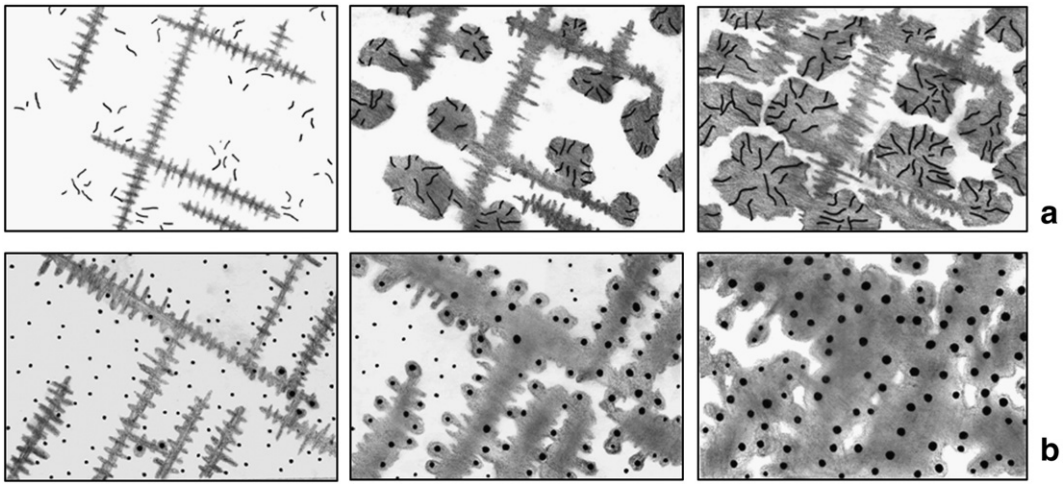

Fig. 13 – Schematic of the eutectic solidification of: (a) flake graphite cast iron; (b) spheroidal graphite cast iron.

[4] Roviglione A, Biloni H. Unidirectional solidification of cast iron: morphological changes of graphite due to in-situ modification. Adv Mat Res 1997;4–5:369–76.
[5] Fraś E, Górny M, López H. Eutectic cell count, chilling tendency and chill in flake graphite cast iron, Part I—theoretical analysis. AFS Trans 2007;115:1–17.
[6] Loper C, Gundlach R. Inoculation, what is it and how does inoculation work? International Inoculation Conference proceedings; 1998. Rosemont Illinois, April 6–8.
[7] Lesoult G, Castro M, Lacaze J. Solidification of spheroidal graphite cast iron I. Physical modeling. Acta Mater 1998;46:983–95.
[8] Nakae H, Jung S, Kitazawa T. Eutectic solidification mode of spheroidal graphite cast iron and graphitization. Proc. of Eighth International Symposium on science and processing of cast iron; 2006. Beijing, China, October 16–19.
[9] Boeri R, Sikora J. Solidification macrostructure of spheroidal graphite cast iron. Int J Cast Met Res 2001;13:307–13.
[10] Rivera G, Boeri R, Sikora J. Solidification of gray cast iron. Scr Mater 2004;50:331–5.
[11] Rivera G, Boeri R, Sikora J. Revealing and characterising solidification structure of ductile cast iron. Mater Sci Technol 2002;18:691–7.
[12] Rivera G, Boeri R, Sikora J. Research advances in ductile iron solidification. AFS Trans 2003;111:1–11.
[13] Rivera G, Boeri R, Sikora J. Influence of the inoculation process, the chemical composition and the cooling rate, on the solidification macro and microstructure of ductile iron. Int J Cast Met Res 2003;16:23–8.
[14] Rivera G, Boeri R, Sikora J. Searching for a unified explanation of the solidification of Cast irons. Proc. of Eighth International Symposium on science and processing of cast iron; 2006. Beijing, China, October 16–19.
[15] Miyake H, Okada A. Nucleation and growth of primary austenite in hypoeutectic cast iron. AFS Trans 1998;106:581–7.
[16] Van de Velde C. A new approach to the solidification of ductile iron. Proc of 1998 Keith D. Millis World Symposium on ductile iron; 1998. South Carolina, USA, October 20–22.
[17] Loper C, Heine R. Dendritic structure and spiking in ductile iron. AFS Trans 1968;76:547–54.
[18] Pedersen K, Tiedje N. Nucleation and solidification of thin walled ductile iron—experiments and numerical simulation. Mater Sci Eng A 2005;413–414:358–62.
[19] Santos H, Sá C. Austenite shell evidence in ductile iron solidification. Int J Cast Met Res 2004;17:319–20.
[20] Randle V, Engler O. Introduction to texture analysis—macrotexture, microtexture and orientation mapping. Taylor & Francis Ltd; 2003.
[21] Diószegi A, Dugic I. The mechanisms of metal expansion penetration in grey cast iron. Proc of Eighth International Symposium on science and processing of cast iron; 2006. Beijing, China, October 16–19.